

## Foam patterning in porous media

Raphail Dautov,<sup>1</sup> Konstantin Kornev,<sup>2</sup> and Valerii Mourzenko<sup>2</sup>

<sup>1</sup>*Department of Numerical Mathematics and Cybernetics, Kazan State University, Lenina Street 18, Kazan 420008, Russia*

<sup>2</sup>*The Institute for Problems in Mechanics, Russian Academy of Sciences, Prospekt Vernadskogo 101, Moscow 117526, Russia*

(Received 16 August 1996; revised manuscript received 21 February 1997)

We consider a model of patterning of one-dimensional foam–bubble chain confined in a bamboolike capillary. The discrete model of such a foam describes a distribution of foam films—lamellae that, like “bridges,” span a capillary. This model is a kind of Ulam map, which admits many metastable distributions of lamellae in a bamboolike capillary as governing parameters (external pressure drop, lattice parameter, lamella tension, and gas compressibility) overcome certain barriers. In particular, some random distributions of bubble sizes over the chain are suited to solutions of the proposed discrete deterministic model. Randomization of lamella positions speaks in favor of the possibility of the glasslike patterning of foam in a bamboolike capillary. For such “chaotic” foam structures, the admissible pressure drop that the bubble chain can sustain, i.e., the so-called start-up, yield pressure drop, rises. We show that the start-up pressure drop depends upon the length of the chain nonlinearly. Only for short chains does it linearly depend upon the number of bubbles in the chain. For infinitely long chains, a saturation effect is observed; i.e., the critical pressure drop becomes independent of the chain length. [S1063-651X(97)13011-2]

PACS number(s): 82.70.Rr, 68.10.-m, 68.90.+g, 05.45.+b

### I. INTRODUCTION

Recent studies [1–12] have shown that foam, because of its unique structure, reduces gas flow in porous media. This blocking effect makes foam a promising blocking fluid for underground gas storage and for other engineering applications [9–11]. To understand the nature of blockage of gas flow by foam, numerous investigators have conducted foam displacement tests in packs of glass beads and etched glass plates [2–4,7–9,12]. It has been shown that, at any given instant of time, foam flows in a small fraction of the pores. The rest of the pores contain “trapped foam,” which effectively blocks the flow. As a result, the permeability to gas is reduced by several orders of magnitude over that which would be assumed with a gas-liquid system without a foaming agent.

In addition to reduction of permeability, foam radically changes the rheological behavior of the gas phase [1–15]. In particular, in the presence of a foam, gas flows as if it were a homogeneous fluid with a start-up yield pressure drop. Such a start-up pressure drop must be applied before foam will move through porous media.

This paper concerns the physical nature of the start-up yield pressure drop. The explanation of the yield pressure drop is usually based upon one fundamental assumption: namely, that foam is incompressible [1,5,10–13]. Let us show that such an assumption leads to a huge capillary barrier.

In explanation of the peculiarities of foam patterning within a porous medium, it is sufficient to consider a one-dimensional foam, i.e., a bubble chain, immersed in a bamboolike capillary. For clarity, we assume that, before deformation, foam films, lamellae, reside in thermodynamically preferential parts of the channel, namely, in each throat where the surface energy of lamellae has a minimum. For such a chain, the distance between adjacent lamellae is on the order of the radius of a pore  $\sim r$ . In this model, the

problem of prediction of the start-up yield pressure drop reduces to a description of how an external pressure is redistributed over the chain.

If we neglect for a time the compressibility of the gas, then to change the pressure by an amount of  $\Delta p$  in a sample with a macroscale  $L$ , we need to overcome the Laplacian capillary barrier  $\Delta p \sim (\sigma/r) \times (\text{number of lamellae})$ , where  $\sigma$  is the tension of individual lamella. Because we have assumed that lamellae reside at each throat, the number of lamellae is proportional to  $L/r$ . Then the capillary barrier is estimated as  $\Delta p \sim \sigma L/r^2$ . It should be noted that, for an absolutely compressible gas, a similar estimate remains in the force. Indeed, for both cases, the total capillary barrier is a sum of the individual Laplacian barriers.

Using this estimate, we conclude that the start-up pressure drop must be giant. The experimental values are significantly lower than this estimate. There are some other additional reasons, based on experimental data, which speak in favor of finite foam compressibility [5,9–11,15]. So this fact should be taken into account.

In this paper, we shall show that the finite compressibility of gas plays an important role in foam patterning and we shall develop a respective theory of foam elasticity that leads to a significantly lower barrier. However, prior to a mathematical analysis, it is useful to point out a range of input physical parameters for which the assumption of foam “incompressibility” (or “absolute compressibility”) may be freely used [14]. Let us consider two characteristic values of pressure perturbations associated with foam in porous media on the microlevel of pores. The first characteristic pressure drop is the Laplacian capillary barrier  $\delta P_c \sim 4\sigma/r$ . It is imposed by the inherent structure of the pore matrix. This is the pressure drop required to push a single lamella through a pore constriction. To estimate the second pressure variation caused by the change of bubble volume, we consider the following imaginary experiment. We displace a single lamella. But other lamellae in the train will remain at their

initial positions at the throats. Then, by treating the gas as ideal, the pressure perturbation within the deformed bubble can be estimated as  $\delta P_g \sim P_g \delta V/V \sim P_g/K$ , where  $V$  is the initial cell volume,  $P_g$  is the initial gas pressure, and  $K$  is an integer number of pores between adjacent lamellae. This pressure variation does not depend on external pressure drop, and it is an inherent characteristic of the foam. It might be expected that whenever  $\delta P_g > \delta P_c$  ( $4\sigma K/P_g r < 1$ ), foam will move as a whole, because in such a case the external pressure drop will be redistributed over the entire system of foam cells. In the opposite case, lamellae are capable of withstanding the variations of pressure of an order of  $\delta P_g$ . This means that the fate of each individual lamella that is able to sustain the local pressure variation of an order of  $\delta P_g$  comes to the forefront and drives the foam patterning. Thus, the above-mentioned inequality assigns a specific meaning for terms of ‘‘compressible’’ or ‘‘incompressible’’ foams and also selects some range of the input parameters within which a theory of foam elasticity can be constructed. The theory of foam elasticity underlies the approach to foam ‘‘plasticity,’’ i.e., the description of a creep of foam lamellae. It should be remembered that, within the framework of the ordinary theory of plasticity, the start-up critical pressure drop can be estimated as a criterion for depinning a dislocation [16]. In this paper, we shall show how such a criterion can be obtained for foams. The mathematical problem is similar to the problem of determining the critical field for vortex formation in Josephson junctions and the like [16–22].

There is another approach to determining the critical pressure drop. It has been proposed by numerous authors [7,10–15]. They treated the critical pressure drop as that required to keep the lamellae moving and, therefore, to overcome the capillary and viscous forces that resist their advance. A detailed investigation into these approaches has been done by Rossen [13,15]. Using this approach, the crucial role in the appearance of the critical pressure gradient has been attributed to the sharp edges, or cusps, within a pore channel, which is modeled as a tube with a periodically varying radius. For a piecewise linear distribution of the pore radius, the channel is formed as a system of frustums of cones. If gas in the cells were incompressible, then some of the lamella positions would be prohibited due to solely geometric restrictions. In this case, the motion of lamellae is considered as a sequence of alternating equilibrium positions of a lamella. For certain shapes of the channel, the bubble has to jump a certain distance in order to conserve volume during the motion. Jumps in lamella position occur when the bubble volume becomes a nonmonotonic function of the lamella position. A channel with edges, or cusps, is such a case. Usually [7,10–15], in order to estimate the critical pressure gradient, the volume-average value of Laplacian pressure drop per bubble is analyzed (provided that the bubble volumes are random and uncorrelated). The volume-average Laplacian pressure drop per lamella represents the net work required to push lamella through the pore. The driving pressure gradient was attributed to the time-averaged value of the pressure drop per bubble. (For steady motion, the relation between time and volume occupied by the bubble is linear.) In such a formulation, the critical pressure gradient in smooth inhomogeneous capillaries, e.g., sinu-

soidal, has to be zero [13]. At the same time, in most experiments on homogeneous bead packs [7,9,12], in which, at a glance, active channels should be smooth, the critical pressure drop was also observed.

In this paper, we develop a nonlinear theory of foam elasticity that casts doubt on the applicability of the mechanism we have just discussed [7,10–15,23]. As it follows from our mathematical analysis, the final results are insensitive to the shape of a pore channel. A more important factor is the ratio  $\delta P_g/\delta P_c$ , which serves as a measure of the binding energy of lamellae with respect to pinning energy. In Sec. II, we formulate the model of foam patterning under a load. Foam is considered as a one-dimensional (1D) chain of lamellae immersed into a bamboolike capillary. It is assumed that, initially, the chain forms a 1D crystal so that the lamellae reside at the channel throats. The model resembles the Ulam model [24,25]. For a small pressure perturbation, it is reduced to the Frenkel-Kontorova model [16,18]. In the two following sections, we discuss two limiting cases of foam: two bubbles, Sec. III, and a continuous chain of bubbles, Sec. IV. In Sec. IV, we demonstrate that the competition between elastic forces caused by the gas compressibility and capillary forces leads to foam coarsening; more precisely, it leads to the possibility of the appearance of superstructures. The discreteness effects result in more complex foam patterning, as follows from Sec. V. In particular, the glasslike ordering is also notable. But the selection of the chain ground state from the thermodynamic principles is difficult, because the resulting equilibrium state of the chain is dictated, in reality, by the history of foam generation and motion through a porous medium. Anyway, numerical analysis shows that the bubble chain in a glasslike state withstands the enhanced pressure drop as compared to that prescribed to crystalline-like ordering. In Sec. VI, we discuss the effect of bubble train length and show that the usual estimate of critical pressure drop  $\nabla p \sim n_b \sigma/r$  [11,23], where  $n_b$  is the linear density of bubbles, is suitable solely for short caravans. For long caravans, the critical pressure drop does not depend on the number of lamellae in the caravan. This effect was first predicted in [26], on the basis of the Frenkel-Kontorova model. It is worth noting that in application to superconductors as described by the mathematically similar model, the importance of the size effect has been pointed out by Lowell [22]. All the conclusions are summarized in Sec. VII.

## II. STATEMENT OF THE PROBLEM IN TERMS OF AN AREA PRESERVING MAP

### A. Assumptions

We shall discuss the nature of foam patterning under the following assumptions.

(1) We shall model the porous medium as a rigid capillary with a radius

$$r = r_0 + \delta \cos\left(\frac{2\pi x}{\lambda}\right). \quad (1)$$

Here  $r_0$ ,  $\lambda$ , and  $\delta$  are some characteristic scales of the porous medium, and the  $x$  axis coincides with the axis of the symmetry of a capillary.

(2) The pore aspect ratio is a low  $\delta \ll r_0 \ll \lambda$ .

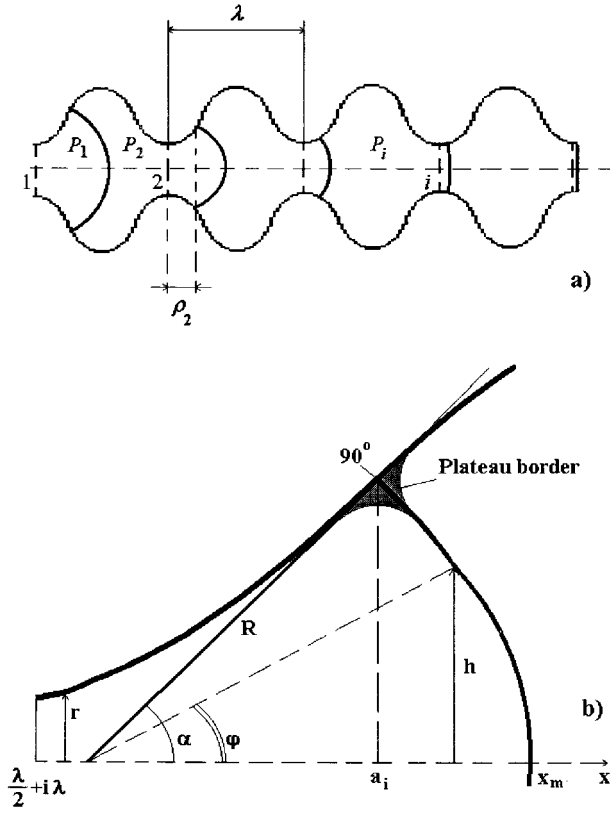


FIG. 1. (a) Scheme of lamella distribution in a wavy channel. Dashed lines are attributed to the initial positions of lamellae, and boldfaced lines represent the lamellae under a load. (b) Specification of the input parameters needed for calculation of the bubble volume variation and capillary force.

(3) In an initial undeformed state, foam is perfectly ordered. Under a load, all the bubbles keep the same mass; i.e., we prohibit the occurrence of diffusion.

(4) The gas in the bubbles is ideal.

(5) One can ignore the Plateau borders and assume that the lamellae intersect the pore walls at  $90^\circ$  angles [8,27].

Assumptions (1) and (2) can be particularly justified by the following arguments. As has been shown experimentally on a homogeneous porous medium [7,28], where the arrangement of the neighboring pore throats is rather regular, the foam transport is realized through some effective sliding channels. These active channels are controlled by the mechanisms for the creation and disappearance of foam lamellae. Frequently, these channels have a slightly varying cross-sectional area [29]. Assumption (2), however, can be altered without any change in most of the physical conclusions. Assumption (3) is stronger, but it allows us to demonstrate the physics of foam patterning in porous media. We particularly relax this assumption in Sec. V. Assumptions (4) and (5) also simplify the model, but they do not play a significant role. A change in the equation of the gas state will merely alter the effective elasticity constants of a foam. But the character of foam behavior will be similar. Assumption (5) has been verified experimentally [8,27].

We turn now to the construction of a model of a bubble chain (Fig. 1). We assume that the train consists of  $N$  lamellae whose centers of chords are prescribed as points  $x = a_1, a_2, \dots, a_N$ . Each lamella undergoes the action of two

kinds of forces: elastic forces and capillary forces. The capillary forces tend to fix the lamellae at the pore throats, while elastic forces, caused by gas compressibility, compel the lamellae to shift into new equilibrium positions. Competition between these forces leads to equilibrium states of the bubble chain.

### B. Elastic forces

We first focus on the elastic response of the bubble chain caused by the gas compressibility. Under a load, the  $i$ th bubble is deformed. And its length, with an accuracy of  $O(\delta/r_0)$ , becomes  $a_i - a_{i-1}$  (see Appendix). The resulting elastic force acting upon the  $i$ th lamella can be written with the same accuracy as

$$f_e = \pi r_0^2 (P_{i+1} - P_i). \quad (2)$$

Here  $P_i$  is the gas pressure within the  $i$ th bubble. Making use of the equation of state of the ideal gas, and accounting for assumption (2), we have

$$P_{i+1}(a_{i+1} - a_i) = P_i(a_i - a_{i-1}) = \dots = P_g K \lambda. \quad (3)$$

Here we denote as  $P_g$  the initial gas pressure in an individual bubble, and  $K\lambda$  is the ‘‘wagon length,’’ i.e., the distance between adjacent lamellae in an initial unperturbed state.  $K$  is an integer number. It is more convenient to rewrite Eq. (3) by introducing a new unknown function,  $\rho_i$ —displacement of the  $i$ th lamella from its initial position at the throat. Then  $a_i = \lambda/2 + \lambda K i + \rho_i$  and Eq. (3) takes the form [30]

$$P_i = \frac{P_g K \lambda}{\rho_i - \rho_{i-1} + \lambda K}. \quad (4)$$

Thus, Eqs. (2) and (4) express the elastic force in terms of the displacements of lamellae.

### C. Capillary forces

To specify the capillary force, consider the membrane analogy. The shapes of curved lamella and the pressure differences across the lamella are dictated by the Laplace formula

$$\Delta P = P_{i+1} - P_i = \frac{4\sigma}{R_i}, \quad (5)$$

where  $\sigma$  is the surface tension,  $2/R_i$  is the sum of the principal curvatures of the  $i$ th lamella, and  $R_i$  is the radius of the spherical membrane. The factor of two accounts for both film interfaces. Rule (5) reflects the thermodynamic drive needed to minimize the surface area of the film. Under a load, some lamellae take positions at which they bulge backward and actually pull the chain forward. Others bulge forward and resist forward displacement. Taking into account assumption (5), we find [see Fig. 1(b)]

$$R_i = r / \sin \alpha(r) \Big|_{x=a_i}, \quad \tan \alpha = \frac{dr}{dx}. \quad (6)$$

Thus, the right-hand side of Eq. (6) is expressed via coordinates of the lamellae in caravan,  $a_i = \lambda/2 + iK\lambda + \rho_i$ , or

through their displacements,  $\rho_i$ . Assumption (2) allows us to write Eq. (6) in the simpler form (Appendix)

$$R_i = \frac{\lambda r_0}{2\pi\delta \sin(2\pi\rho_i/\lambda)}. \quad (7)$$

Then the capillary force can be written with an accuracy of  $O(\delta/r_0)$  as

$$f_c = \pi r_0^2 \frac{4\sigma}{R_i}, \quad (8)$$

where  $R_i$  is expressed by Eq. (7).

The balance of forces, Eqs. (2) and (8), gives us the desired equation

$$P_{i+1} - P_i = -\frac{8\pi\delta\sigma}{\lambda r_0} \sin\left(\frac{2\pi\rho_i}{\lambda}\right). \quad (9)$$

To specify completely the state of this chain, the system of Eqs. (4) and (9) should be subjected to boundary conditions for the zeroth and the last  $N-1$  lamellae as

$$P_0 = P_g P_{\text{ext}}, \quad P_N = P_g P, \quad (10)$$

where  $P_{\text{ext}}$  and  $P$  are the external dimensionless pressures applied to the chain.

### C. Thermodynamic potential

Thus, all the states of the chain undergoing a load are described by Eqs. (4), (9), and (10). At the same time, as will be shown below, the above formulated problem allows few solutions at some range of the input physical parameters. The required essential property of the model is that its energy in a ground state has to be at a minimum. The extremity of the energy could yield a metastable lamella distribution that is also interesting for applications. The energy of the chain of  $N$  bubbles consists of two parts: namely, the elastic energy  $E_e$  and the surface energy  $E_c$  of lamellae

$$F = E_e + E_c. \quad (11)$$

The surface energy  $\Delta E_{ci}$  accumulated by the  $i$ th lamella is equal to the work of capillary forces  $4\pi\sigma r_0^2/R_i$  during the lamella displacement

$$\Delta E_{ci} = \int \frac{4\sigma\pi r_0^2}{R_i} d\rho_i = 4\sigma\pi r_0\delta \cos\frac{2\pi\rho_i}{\lambda}.$$

The elastic energy  $\Delta E_{ei}$  of the  $i$ th bubble, associated with bubble stretching, is defined as

$$\Delta E_{ei} = - \int P_i(V_i) dV_i = \pi r_0^2 P_g K \lambda \ln \frac{P_i}{P_g}.$$

Here we have used Eq. (4) in order to calculate the integral.

The work of the bubble chain against external pressures is equal to

$$\pi r_0^2 P_g (P\rho_{N-1} - P_{\text{ext}}\rho_0).$$

Then the total thermodynamic potential of the system per lamella is expressed as

$$F = \frac{\pi r_0^2 P_g K \lambda}{N} \sum_{i=1}^{N-1} \ln \frac{P_i}{P_g} - \frac{4\pi r_0\sigma\delta}{N} \sum_{i=0}^{N-1} \cos \frac{2\pi\rho_i}{\lambda} + \frac{\pi r_0^2 P_g}{N} (P\rho_{N-1} - P_{\text{ext}}\rho_0). \quad (12)$$

### D. Reverse problem

It is convenient to rewrite all the equations in their dimensionless form. We use the following normalization:

$$2\pi \frac{\rho_i}{\lambda} \rightarrow \rho_i, \quad \frac{P_i}{P_g} \rightarrow p_i, \quad \frac{2F}{P_g \lambda r_0^2} \rightarrow F.$$

Then Eqs. (4), (9), (10) take a form of the map

$$p_{i+1} - p_i = -2\pi\mu \sin\rho_i, \quad (13)$$

$$p_{i+1} - \rho_i = \frac{2\pi K}{p_{i+1}} - 2\pi K, \quad (14)$$

$$p_0 = P_{\text{ext}}, \quad p_N = P, \quad (15)$$

in which the parameter

$$\mu = \frac{4\sigma\delta}{P_g r_0 \lambda}$$

serves as a measure of the intensity of capillary forces with respect to the elastic forces. We also rewrite the energy by expressing  $\rho_{N-1}$  in Eq. (12) through  $p_i$  and  $P$  and by solving Eq. (14) recursively. Then the thermodynamic potential takes the following dimensionless form:

$$F = \frac{2\pi K}{N} \left\{ \sum_{i=1}^{N-1} \left( \ln p_i + \frac{P}{p_i} \right) - \frac{\mu}{K} \sum_{i=0}^{N-1} \cos\rho_i \right\} + \frac{(P - P_{\text{ext}})\rho_0}{N}. \quad (16)$$

The mathematical model (13)–(16) is suitable for analysis in a wide spectrum of physical problems related to 1D foam patterning and, in particular, to predictions of foam texture. We, however, recall that the goal of our study consists in the prediction of the critical pressure drop required to shift the bubble train as a whole. In the formulation of the map (13)–(15) and in minimization of Eq. (16), the critical pressure drop has not been specified. Therefore, we are going to determine some additional criteria that select the desired solution to map (13)–(16).

We turn now to the physical picture of the displacement of the bubble train. It should be remembered that whenever the last lamella is free, i.e.,  $P=1$ , there is a single pinning force—a capillary force—which tends to keep the last ( $N-1$ )st lamella at an equilibrium position. Moreover, this force resists forward displacement only within the period  $\rho_{N-1} \in [0, \lambda/2]$ , where the lamella bulges forward. Within this period, the profile of this force has a single extreme point—the maximum [see Eqs. (7) and (8)]. Therefore, it

might be expected that the bubble train begins motion immediately after the last lamella has reached the extreme point. The pressure drop required to overcome this barrier will be called the critical pressure drop,  $G = P_{\text{ext}} - 1$ . Precisely speaking, if the dependence  $G(\rho_{N-1})$  is nonmonotonic, the maximum of possible  $G(\rho_{N-1})$  within the period  $0 < \rho_{N-1} < \lambda/2$  should be called the critical pressure drop. For this reason, the solution of the boundary value problem is replaced by the solution of the Cauchy problem: the knowledge of  $P = 1$  and  $\rho_{N-1}$  determines recursively  $p_i$  and  $\rho_i$  for all  $i$ . Then Eqs. (13) and (14) define such a map  $T$  that a point  $U_{i+1} = (p_{i+1}, \rho_{i+1})$  is transformed into point  $U_i = T(U_{i+1}) = (p_i, \rho_i)$ . One can check by direct calculations that the Jacobian matrix of  $T$  has a unit determinant. Hence the map is area preserving. This map, usually called the Ulam map, has been previously discussed in a different context and statement [24,25]. Within the framework of the problem of foam patterning, we seek the relation of  $P_{\text{ext}} = P_{\text{ext}}(\rho_{N-1})$ , where the parameter  $\rho_{N-1}$  is used to distinguish different solutions to Eqs. (13) and (14). Then we determine the maximum pressure drop among those calculated. The goal of this study consists in solving the reverse problem, i.e., the prediction of critical pressure drop as a function of the input parameters. It is difficult to find the explicit solution to the general case. We therefore consider some asymptotes. The linear version of the model in Eqs. (13)–(15), i.e., asymptotes  $\rho_i \rightarrow 0$ ,  $P_{\text{ext}} \rightarrow 1$ , allows us to select distinguishing limiting cases of foam patterning.

### E. Correlation length

Consider the semi-infinite chain  $N \rightarrow \infty$ . Then the solution to the corresponding linearized problem

$$\begin{aligned} p_{i+1} - p_i &= -2\pi\mu\rho_i, \\ \rho_{i+1} - \rho_i &= -2\pi K p_{i+1}, \\ p_0 &= P_{\text{ext}} - 1, \quad p_N = 0 \end{aligned}$$

can be written in the form [31]

$$\rho_i = a e^{-\omega i},$$

where  $a$  is a constant defined by the boundary conditions and  $\omega$  satisfies the following transcendental equation

$$\cosh\omega = 1 + 4\pi^2 K\mu. \quad (17)$$

Parameter  $N_{\text{cor}} \sim 1/\omega$  can be called the correlation length. But it is better to call this parameter the screening length because it defines the characteristic distance over which the pressure in the bubbles decreases from  $P_{\text{ext}}$  to 1.

In regimes where colligative properties of foam play the crucial role, the parameter  $K\mu$  is less than one (see Introduction), and the screening length of a caravan is estimated as

$$N_{\text{cor}} \sim \frac{1}{2\pi\sqrt{K\mu}}, \quad K\mu \ll 1. \quad (18)$$

In the opposite case,

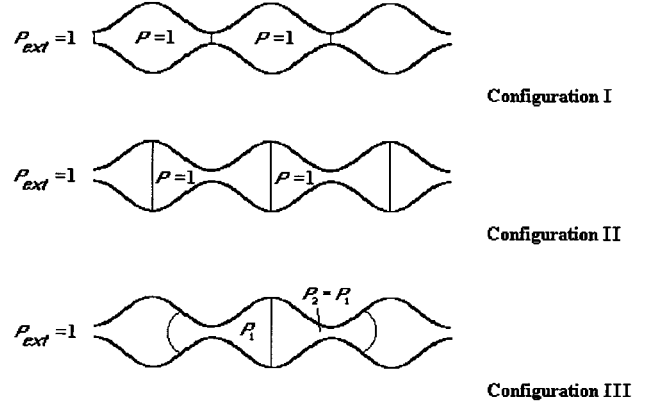


FIG. 2. Configurations I and III are the two possible equilibrium states of two bubbles. Configuration II is unstable.

$$N_{\text{cor}} \sim \frac{1}{\ln(2 + 4\pi^2 K\mu)}, \quad K\mu \gg \frac{1}{4\pi^2}. \quad (19)$$

Thus, in the former case, the load is distributed over a large number of lamellae. In the last case, the small number of first lamellae bear the main load. Therefore, one expects that a continuous approximation of model (13)–(16) appropriately describes the characteristic feature of the foam patterning, whenever  $K\mu \ll 1$ , and contrarily, the discrete effects should be taken into account for cases where  $K\mu \geq 1/4\pi^2$ .

### III. TWO BUBBLES

Even for two bubbles, the above formulated problem is nontrivial. So we start from the analysis of this simple example: a short chain consisting of two bubbles.

We begin with a description of possible equilibrium unloaded states of such a chain. One can easily find two trivial solutions of Eqs. (13) and (14) that satisfy the boundary condition  $P_{\text{ext}} = P = 1$ . The first represents the state in which all the lamellae reside in the throats of the channel. In the second case, the lamellae are attached at the widest part of the pore (configurations I and II in Fig. 2, respectively). Configuration I is stable with respect to small perturbations in the lamella positions, because the lamella bulges forward, and its further displacement is hindered. In configuration II, small perturbations in the lamella positions, caused by the gas pressure perturbations within bubbles, result in the appearance of a capillary force codirected with pushing force. Also, in configuration II, the surface energy of lamellae rises, while the elastic energy remains the same as that in configuration I. Consequently, this configuration is unstable.

If we contract both bubbles and then make them free, then it is possible, in principle, that capillary forces acting upon the external lamellae will be large enough to keep increased pressure in the bubbles. The corresponding steady configuration III, which satisfies Eqs. (13) and (14) and boundary conditions  $P_{\text{ext}} = P = 1$ , is shown in Fig. 2. Now the state of the middle lamella is quite stable, because small perturbations of pressure within the bubbles cause a restoring effect. Making use of Eqs. (13) and (14), we obtain the pair  $(\rho, p)$  by solving the following equations:

$$p = 1 + 2\pi\mu \sin\rho, \quad (20)$$

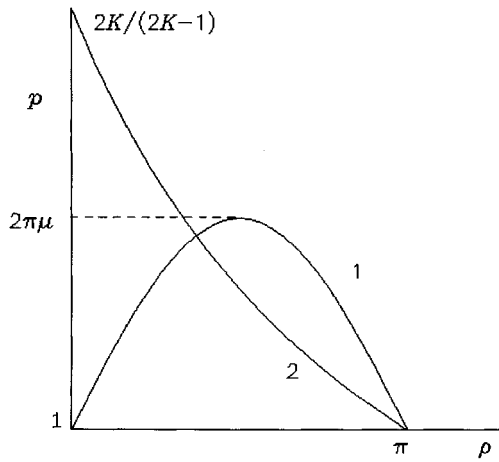


FIG. 3. Scheme for graphic solving Eqs. (20) (curve 1) and (21) (curve 2). The solution first appears as the curves touch one another.

$$p = \frac{2\pi K}{\rho - \pi + 2\pi K}, \tag{21}$$

where  $p$  denotes the pressure within the bubbles, and  $\rho$  is the displacement of the end lamellae  $\rho = 2\pi - \rho_1 = \rho_3$ . The solvability condition of Eqs. (20) and (21) (see Fig. 3) demands that

$$\left. \frac{dp}{d\rho} \right|_{\rho=\pi}^{\text{Eq. (20)}} < \left. \frac{dp}{d\rho} \right|_{\rho=\pi}^{\text{Eq. (21)}}.$$

Here the upper index means that the derivatives have to be calculated by making use of the respective formula. Using simple algebra, we find the solvability condition in the form

$$K\mu > \frac{1}{4\pi^2}. \tag{22}$$

In other words, configuration III cannot be realized if the capillary forces are small or the bubble length is small.

Proceeding to the analysis of the possible range of  $P_{\text{ext}}(\rho_3)$ , we find that two distinguishing regimes of chain behavior take place [Fig. 4(a)]. They are distinguished by the parameter  $K\mu$ . The first regime corresponds to  $K\mu < 1/4\pi^2$ , when all the lamellae reside in the vicinity of the throats. As parameter  $K$  rises, novel configurations such as configuration III appear. In other words, lamellae are capable of occupying the ‘‘dangerous’’ positions at the widest part of the pore, whenever  $K\mu > 1/4\pi^2$ .

Figure 4(a) shows the pressure  $P_{\text{ext}}$  as a function of the displacement  $\rho_3$  for bubble trains with  $N=3$  and  $\mu K \sim 0.008 < 1/4\pi^2$ . For each  $P_{\text{ext}}$  there are two equilibrium states of the train. Two points,  $(P_{\text{ext}}=1, \rho_3=0)$  and  $(P_{\text{ext}}=1, \rho_3=\pi)$ , represent configurations I and II, respectively. The characteristic plot of energy  $F$  versus  $P_{\text{ext}}$  is depicted in Fig. 4(b). This plot can be subdivided into three pieces: two branches before the intersection point and the loop in the vicinity of the maximum of  $P_{\text{ext}}$ . The lower branch of curve  $F(P_{\text{ext}})$  before the loop corresponds to an increasing branch of  $P_{\text{ext}}(\rho_3)$ . These states can be obtained from the initial

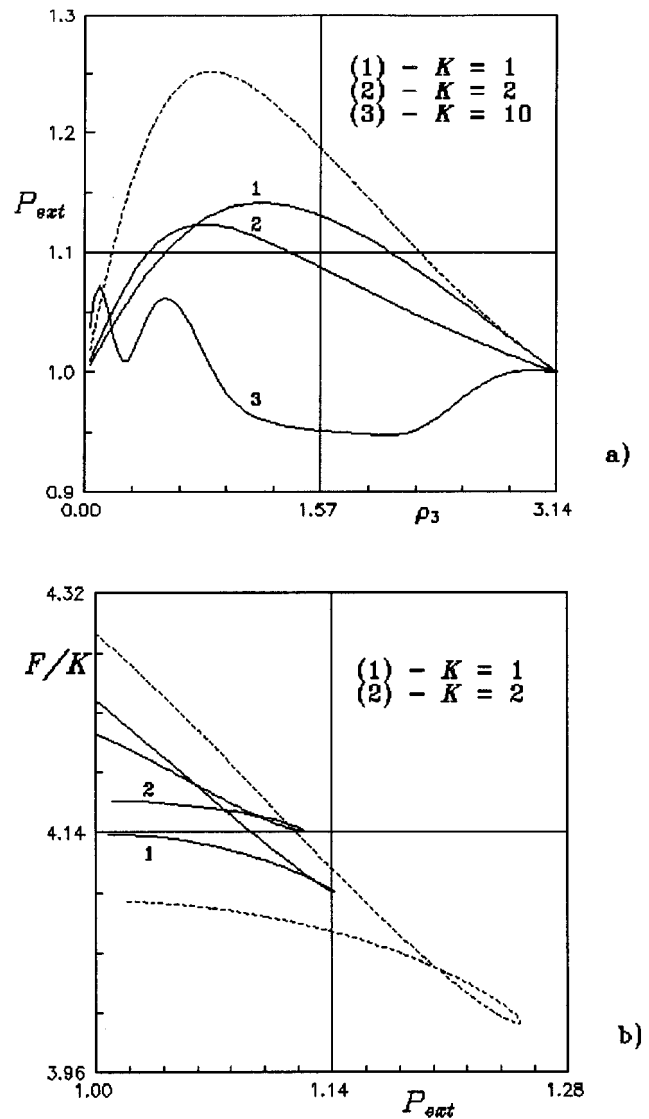


FIG. 4. (a) Admissible external pressure and (b) respective energy per bubble for two bubbles,  $\mu=0.008$ ; the dashed line corresponds to parameters  $\mu=0.016, K=1$ .

undeformed states by slowly and continually increasing the external pressure. We shall call such a process the ‘‘adiabatic’’ variation of  $P_{\text{ext}}$ . In the vicinity of the maximum of the admissible external pressure, the energy behaves non-monotonically. The corresponding states with a minimum energy cannot be reached adiabatically. In order to obtain such states, we have to consider some dynamic process of loading. The upper branch of  $F(P_{\text{ext}})$  after the loop corresponds to the descending branch of  $P_{\text{ext}}(\rho_3)$ . These states are mechanically stable and can be considered as a realization of some dynamic process.

Comparison of curves 1 and 2 in Fig. 4(a) shows that, for  $K=2$ , the admissible maximum pressure  $P_{\text{ext}}$  decreases relative to the case in which  $K=1$ . For larger  $\mu$ , the bubble train withstands the larger pressure  $P_{\text{ext}}$  [Fig. 4(a)]. This means that the maximum pressure increases with the effective pinning force, which is ruled by both the capillary force and effective bubble compressibility.

Further increasing the length of the bubble,  $K$ , we arrive

at the range  $\mu K > 1/4\pi^2$ . Figure 4(a) demonstrates the behavior of the function  $P_{\text{ext}}(\rho_3)$  for the case in which  $K = 10$ ,  $\mu = 0.008$ . This is typical behavior. For the large lattice parameter,  $K = 10$ , there are four solutions for each  $P_{\text{ext}} > 1$  in the range  $\rho_3 < 1$ . The number of peaks depends upon the relation between the effective compressibility of a bubble and the magnitude of capillary force through parameter  $K\mu$ . On the other hand, for  $\rho_3 \sim 1$ , curve  $P_{\text{ext}}(\rho)$  intersects line  $P = 1$ . This fact indicates the presence of configuration III.

Thus, the simple model demonstrates the highly nonlinear character of foam patterning even for two bubbles. It might be expected that colligative properties will come to the forefront with the growth of bubble population.

#### IV. CONTINUOUS MODEL

In this section, we shall discuss the characteristic features of another limiting case—a continuum chain. Going over from a discrete variable to a continuous variable,  $s = 2\pi Ki$ , we rewrite Eqs. (13) and (14) as

$$-\frac{dp}{ds} = \frac{\mu}{K} \sin \rho, \quad (23)$$

$$\frac{d\rho}{ds} = \frac{1}{p} - 1, \quad (24)$$

One expects that the continuous model, Eqs. (23) and (24), approximates the discrete one, whenever  $p_i$  and  $\rho_i$  slowly vary with  $i$ . Quantitative estimates of the limits of the validity of the continuous model have been done in Sec. II E.

The system (23) and (24) has the first integral

$$\ln p - \rho = E + \frac{\mu}{K} \cos \rho, \quad (25)$$

where  $E$  is a constant that depends on boundary conditions. The analysis of the system of equations [(23) and (24)] allows us to clarify the main peculiarities of the inherent structure of the bubble chain in relation to the magnitude of parameter  $E$ . By virtue of the translational symmetry  $\rho \rightarrow \rho + 2\pi n$ ,  $n = 0, \pm \infty$  (overbar denotes an inclusive range), the system of equations [(23) and (24)] may be considered within the whole range of  $\rho \in (-\infty, \infty)$ . It follows from the phase portrait (Fig. 5) that the system has two kinds of singular points: hyperbolic and elliptic singular points. Points  $p = 1$ ,  $\rho = 2\pi n$ ,  $n = 0, \pm \infty$  serve as hyperbolic singular points. These singular points represent the solutions describing configuration I in Fig. 2. Lamellae are attached to the thinnest parts of the channel so that the surface energy of lamellae has a minimum. Points  $p = 1$ ,  $\rho = \pi(2n + 1)$ ,  $n = 0, \pm \infty$  are elliptic. They describe configuration II in Fig. 2. Lamellae tend to leave these wide parts of the channel because the surface energy takes the highest possible value here. The hyperbolic points are connected by a separatrix, which has two branches within each cell of a symmetry of the phase portrait. One of them exits from the left point, then passes above line  $p = 1$ , and enters to the right hyperbolic point. The other branch goes in the opposite direction under line  $p = 1$ . The separatrix is described by the transcendental equation

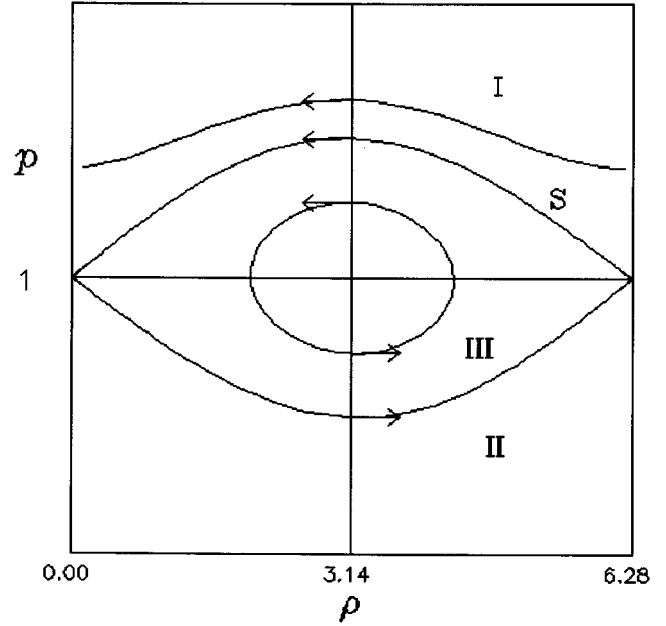


FIG. 5. Phase portrait of the system (23) and (24). The separatrix is denoted as  $S$ . Arrows show the direction of the increasing arclength  $s$ .

$$\ln p - p + 1 = \frac{\mu}{K} (\cos \rho - 1), \quad (26)$$

which follows from Eq. (25). We denote parameter  $E$  at the separatrix as

$$E = E^{**}, \quad E^{**} = -1 - \frac{\mu}{K}. \quad (27)$$

The phase plane  $(P, \rho)$  is subdivided by the separatrix into three parts. Upper part I and lower part II represent “infinite motion” ( $E < E^{**}$ ) of the test point, while the internal part III envelopes all the curves of “finite motion” ( $E > E^{**}$ ). All integral curves within domain III pass through points at which  $p_N = 1$ . So they describe the bubble trains with free, i.e., unloaded, boundary lamellae. The integral curves of domain I illustrate a different physical situation—a contracted bubble train with blocking lamella  $\rho_{N-1} = 0$ ,  $p_N > 1$ . Similarly, extended bubble trains with fixed boundary lamella  $\rho_{N-1} = 0$ ,  $p_N < 1$  are represented by domain II. Each of the singular points  $p = 1$ ,  $\rho = 2\pi n$  creates four branches of separatrix—the entering branches and the exiting ones. The respective solutions correspond to distinguishing configurations of the chain. Therefore, if some “realization of the separatrix” will incorporate a single or a few singular points, then the respective texture of the train will be complex. If we designate the current number of lamellae as time, then the finite motion in domain III can be treated as a motion with a finite time period  $T$ . This means that the number of bubbles accumulated by a single cycle of revolution of an integral curve is a finite value. When the solution approaches the separatrix, period  $T$  tends to infinity; i.e., the solution describes an unconfined bubble train. The solution also demonstrates the effect of the “irreversibility” of the bubble train displacement. Namely, after the action of critical pressure

drop has ended, part of the lamellae never occupy former positions. The solution looks like the solitary “domain wall” [16,18,26]:

$$\rho = 4 \tan^{-1} \exp[-(x-x_0)] + O\left(\sqrt{\frac{\mu}{K}}\right), \quad x = \sqrt{\frac{\mu}{K}} s. \quad (28)$$

That is, under the given pressure drop, all the lamellae behind of the “wall” at left infinity  $s \rightarrow -\infty$  shift to the period  $\rho = 2\pi$  and reside there after unloading. Lamellae at right infinity  $s \rightarrow \infty$ , ahead of the wall, keep the undeformed state  $\rho = 0$ . The domain wall matches the second zone (the undisturbed zone) where the lamellae are pinned at the equilibrium state with the first zone, where lamellae are displaced over the period of channel. The wall size can be estimated in an order of magnitude as  $O(\lambda\sqrt{K}/\sqrt{\mu})$  [26].

The domainlike structure resembles configuration III in Fig. 2. But the similarity is not complete because the effect of the ensemble of the lamellae plays a crucial role in foam patterning within the framework of the continuous model. The collective interactions of lamellae guarantee the stability of domainlike structures in the whole range of  $K\mu$ , where the continuous model is valid. This behavior absolutely differs from that of two bubbles [recall that inequality (22) selects the range of  $K\mu$  at which configuration III exists].

The passage to the continuum limit enables us to be persuaded that the pressure variation is finite for all solutions we are interested in (domain III). The upper boundary for the admissible pressure drop is expressed by the maximum of the separatrix. By analyzing Eq. (26), we find that the maximum pressure at the separatrix is prescribed as  $\rho = \pi$ . Inserting this value into Eq. (26), we arrive at the following equation:

$$\ln(1+G) - G + \frac{2\mu}{K} = 0. \quad (29)$$

Equation (29) expresses the magnitude of the critical pressure drop  $G$  as a maximum point of the separatrix.

The general conclusion of this study is that the bubble train is unable to sustain the pressure drop overcoming the threshold  $G$ , provided that one of the train ends is free.

Analysis of the cyclic solutions from domain III shows that any integral curve gives rise to an infinite number of solutions of the system of Eqs. (23) and (24) (provided that the number of lamellae  $N$  in the train is successively increased, but the external pressure drop remains unchanged at  $P_{\text{ext}} \leq 1+G$  level). This means that, for any given  $N$ , there are several solutions to Eqs. (23) and (24) with the same  $P_{\text{ext}}$  (Fig. 6). Each of the solutions is characterized by the distinguishing input parameters  $\rho_{N-1}$  and  $E$ . Since we are interested in the start-up pressure drop, only the adiabatic solution [curve I in Fig. 6(b)] seems to be suitable.

## V. DISCRETE MODEL

The continuous model, Eqs. (23) and (24), is valid whenever lamellae displacements and pressure vary slightly over the train. This assumption is valid for trains with small  $\mu$  and moderate lattice parameters  $K$ ; or, more precisely, until the

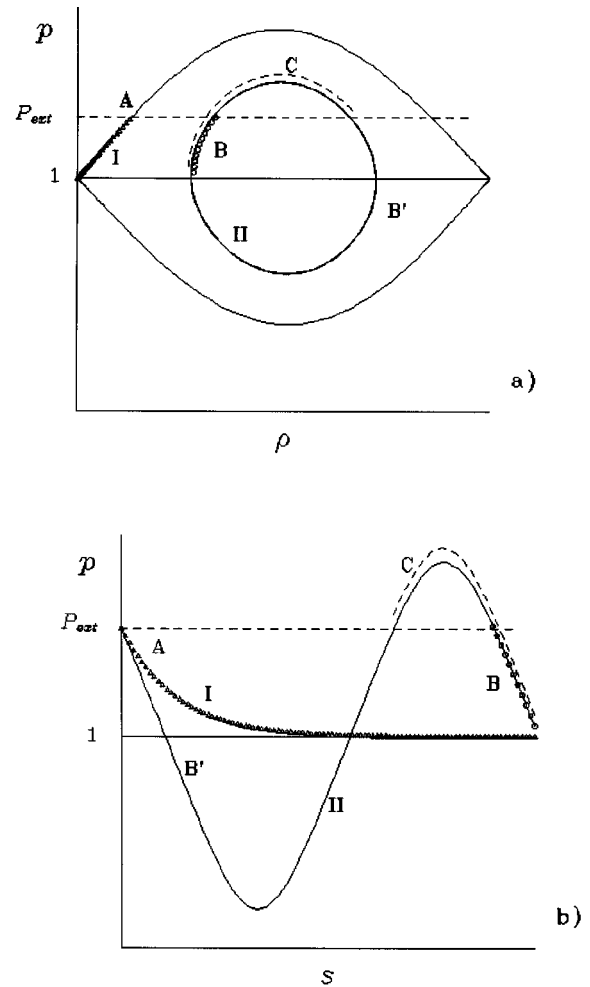


FIG. 6. Multivariacy in choosing the appropriate solution of Eqs. (23) and (24). (a) The scheme of the path in phase portrait, (b) the typical shape of corresponding solution. Parameter  $s$  is counted from arbitrary starting points to demonstrate the characteristic feature of the dependences prescribed to the distinguishing branches. Curve II makes a single full revolution, starting from the bold dot and entering point  $B$ .

collective effects prevail over the individual feature of each bubble (see Introduction and Sec. III E). The intermediate regime is important for applications and, what is more interesting, one expects that the analysis of the discrete model (13)–(15) will be able to select quantitatively the different regimes of the foam behavior and predict novel solutions. As mentioned above, the well-known Ulam model [24,25] contains some characteristic features of the model under consideration. The main result lies in the fact that the Ulam map has stochastic solutions that lie within stochastic domains, separated by domains of regular solutions [25]. All the trajectories, starting from the vicinity of hyperbolic point  $\rho = 0, p = 1$ , belong to stochastic layer IV in Fig. 7. The stochastic layer is separated by regular trajectories from the upper and lower regions of regularity. Near the elliptic singular point  $\rho = \pi, p = 1$ , there is a “stability island” separated from the stochastic layer by a cyclic regular trajectory. The island is termed stable due to its mechanical sense, i.e., an island in which the test point moves regularly.

In our case, this island in the phase portrait carries another

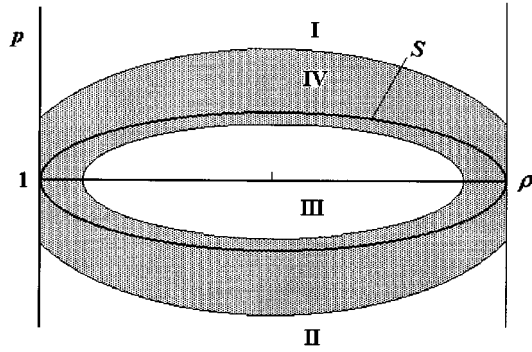


FIG. 7. The sketch of stochastic layer IV of map (13) and (14) at the separatrix "S."

meaning. Any solutions from the vicinity of elliptic singular points describe such a distribution of lamellae whose bubbles are slightly stretched or contracted. But all the lamellae remain at the widest part of the pore. Surface energy of lamellae for these solutions is enhanced with respect to the ground state. Therefore, the lamellae most likely jump through these "dangerous" points. One expects that the equilibrium state of the train, which is established with time in a dynamic way, cannot include such "dangerous" pieces. In other words, any trajectory that starts within the stochastic layer does not penetrate the island. Such an island exists until the capillary pressure and bubble compressibility exceed a certain critical value expressed by inequality [24,25]

$$\mu K > \frac{1}{\pi^2}. \quad (30)$$

Inequality (30) resembles inequality (22) and ensures the possibility of the appearance of configurations like configuration III in Fig. 2. As soon as the input parameters get into a range satisfying the inequality (30), the elliptic singular point becomes unstable and the island disappears. Some bubble trains with a single free end may contain the domains where lamellae reside close to the widest part of the pore. The pressure within such bubbles remains on the order of the initial undisturbed level. Despite the evident instability of local parts of the train, the caravan as a whole might be quite stable. This happens due to the high bubble compressibility or strong capillary pinning: the individual fate of the bubbles comes to the forefront while the collective events lose actuality in the sense mentioned in Sec. II E, Eq. (19).

Figure 8 shows the typical curve  $P_{\text{ext}}(\rho_{N-1})$  for long trains. Here  $N=101$ . The plot reveals the quasiperiodic dependency, Fig. 8(a), which has already been discussed for the continuous model (Sec. IV). In the description of the steady equilibrium state of the bubble train, we start with the pair  $(\rho_{N-1}, 1)$ ,  $\rho_{N-1} \rightarrow 0$  and use map  $T$ . The expected result, based on the analysis of the continuous model (Sec. IV), is that the trajectory is unable to overcome the barrier (separatrix). But the discrete picture is more complex. Namely, when displacement  $\rho_{N-1}$  becomes nearer to zero beyond a certain critical value, chaotic behavior replaces the regular one, Fig. 8(b). This means that the corresponding trajectories of solutions to Eqs. (13) and (14) pass through the stochastic layer IV on the phase plane (Fig. 7). The randomization of the lamella distribution speaks in favor of the glasslike pat-

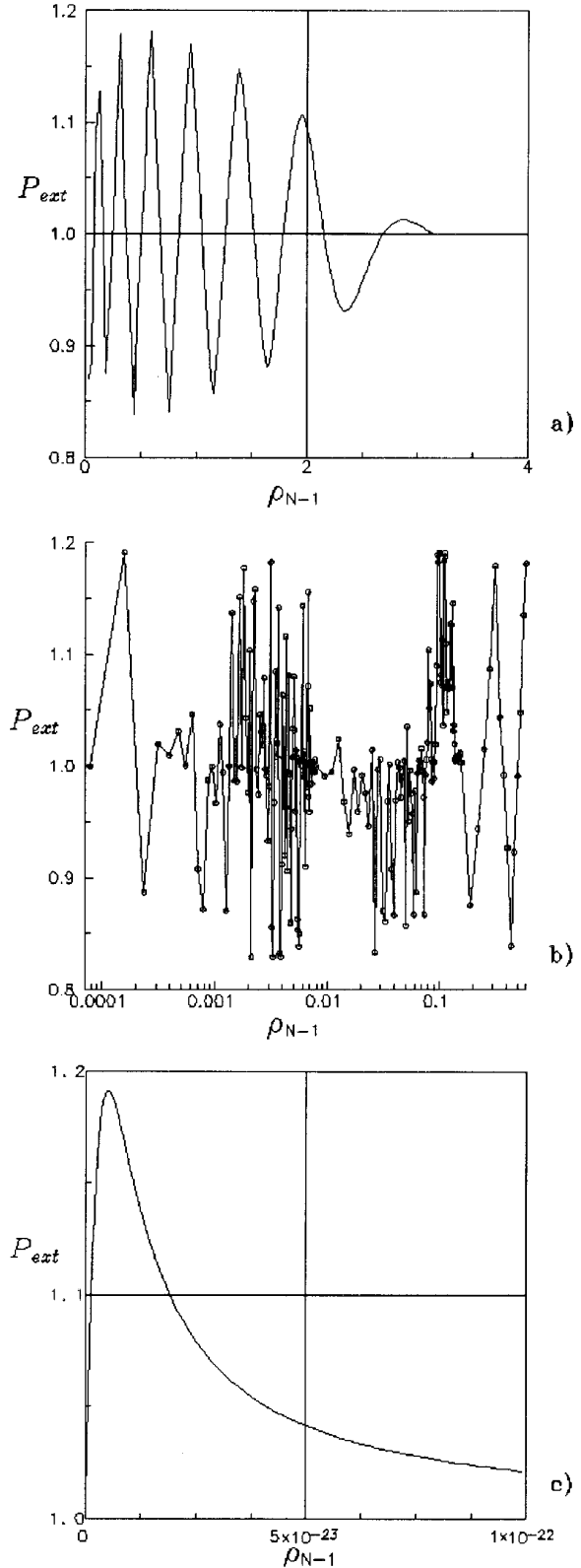


FIG. 8. The external pressure  $P_{\text{ext}}$  in different resolutions of  $\rho_{N-1}$ ,  $\mu=0.008$ ,  $K=1$ ,  $N=101$ .

tering of foam. However, with further decreasing the displacement of last lamella  $\rho_{N-1}$ , a regular part of  $P_{\text{ext}}(\rho_{N-1})$  was found once more, Fig. 8(c). This is associated with the regime of the regularity of the map.

The energy  $F$ , as a function of  $\rho_{N-1}$ , is presented in Fig.

9. From this figure, we see that the solutions for trains with  $N=101$  and minima  $F$  correspond to small displacements of the last lamella,  $\rho_{N-1}$ . On the other hand, the randomization of the bubble train is observed [Fig. 9(b)] within the same range of the displacements of the last lamella as that in Fig. 8(b). When the last lamella closely tends to the throat,  $\rho_{N-1} \rightarrow 0$ , a regular part of the energy  $F(\rho_{N-1})$  is displayed, Fig. 9(c). The characteristic feature of foam behavior with a different ordering is demonstrated by Figs. 10 and 11.

A detailed analysis of pressure and energy dependencies shows that there are several intervals of the displacements of the last lamella within which the energies of the chain vary slightly between the different states. It is very difficult to distinguish such increments numerically. Figure 11 shows the phase portrait, pressure, and displacement distributions for the three states marked in Fig. 10(a). Points  $A$ ,  $B$ , and  $C$  have the same  $P_{\text{ext}}$ . The two solutions  $A$  and  $B$ , prescribed as increasing and decreasing branches of the curve in Fig. 10(a), trace almost the same trajectories and accumulate the similar domains of the compressed and extended bubbles, Fig. 11(a). The trajectory  $C$  describes another solution and contains a train structure different from that of  $A$  and  $B$ , Fig. 11(b).

The complexity of the foam texture can be revealed by analyzing the number of domains in the train. We use here the term ‘‘domain’’ in order to distinguish the region within which the displacements of the lamellae are almost constant, Fig. 11(c). In our numerical experiments, we found that the states with more complex structure, containing several domains of extended or compressed bubbles, may have a smaller energy than those that have fewer domains. This is contrary to the tendency that has been observed in the region of the regular solutions of Eqs. (13) and (14), where the greater the number of domain walls, the larger the energy [cf. Figs. 8(a) and 9(a)].

The variation of the number of domains  $N_D$  in the bubble chains is represented in Fig. 12. The number  $N_D$  gradually increases with  $\rho_{N-1}$ , but relation  $N_D(\rho_{N-1})$  is not regular.

The obtained results show that the solution to the problem of the selection of the ground state in the case of long bubble train  $N \rightarrow \infty$  is very complex. We observe the high sensibility of the solutions of Eqs. (13) and (14) with respect to  $\rho_{N-1}$  whenever the physical parameters vary within the domain of stochasticity. Within the family of input parameters under consideration, states with the same boundary pressure  $P_{\text{ext}}$  differ in energies only slightly and may be considered as equivalent.

One can take another criterion of the choice of the ground state of a bubble chain under given pressure  $P_{\text{ext}}$ . This is the ‘‘adiabatic’’ criterion. We already discussed that criterion in Sec. III. It can be obtained by variation of the initial lamella positions under slow continuous variation of the pressure  $P_{\text{ext}}$ . This configuration has the smallest  $\rho_{N-1}$ , among other states with the same  $P_{\text{ext}}$ , and the simplest domain structure,  $N_D=1$ .

Within the framework of the ‘‘adiabatic’’ criterion, the maximum pressure drop  $G$  is estimated by using the relation between  $P_{\text{ext}}$  and  $\rho_{N-1}$ , near the first maximum. This is the smallest estimate, because we expect the onset of motion as soon as the applied pressure drop overcomes this criterion.

Figure 13 demonstrates the first maximum pressure  $P_{\text{ext}}(\rho_{N-1})$ , which we observed in the range  $\rho_{N-1} \rightarrow 0$  for various  $\mu$  and  $K$ . One can see that, for a small  $\mu$  and  $K$ , the maximum admissible pressure is well predicted by the continuous model, Eq. (29). When  $\mu$  or  $K$  increase, the prediction of the continuous model underestimates the admissible pressure. This can be explained by the fact that a solution of Eqs. (13) and (14) follows an integral curve of Eqs. (23) and (24) only approximately. Indeed, from the Eq. (13),  $p_{N-1}$  is expressed as

$$p_{N-1} = 1 + 2\pi\mu \sin\rho_{N-1}. \quad (31)$$

By comparing Eq. (31) with Eq. (26), we obtain that whenever condition (22) is satisfied, point  $(\rho_{N-1}, p_{N-1})$ ,  $\rho_{N-1} \ll 1$  rises above the separatrix, Eq. (26), on the phase plane. The difference between the integral curves for a discrete model and a continuous one increases with the growth of  $\mu$  and  $K$ . The critical values of  $\mu$ , defined by Eq. (22), are shown by arrows in Fig. 13 for each curve. It can be seen that Eq. (22) may be considered as a limit for the validity of the predictions of the continuous model.

When  $\mu K$  approaches  $1/\pi^2$ , the discreteness of the system of Eqs. (13) and (14) becomes substantial. Its solutions, with a small  $\rho_{N-1}$ , become sensitive to the variation of the initial data. And various chaotic phenomena can be observed. The trajectories of the stochastic solutions belong to a stochastic layer and go in the vicinity of the separatrix of the continuous system of Eqs. (23) and (24). The chaotic features of these solutions may be attributed to two main effects. First, the variations of initial data  $\rho_{N-1}$  are able to abruptly alter the branch of the separatrix along which trajectories are passing. Second, the distribution of points along the trajectory is also sensitive to the initial data: while the domains might occupy various regions, the associated energy remains at almost the same level. Figure 14 demonstrates the inherent structure of the phase portrait, associated with the glasslike patterning of foam. The main conclusion is that the admissible external pressure rises as the bubble train acquires the glasslike structure.

## VI. EFFECT OF THE TRAIN LENGTH

The analysis of the steady states of bubble chains has shown that the applied pressure drop penetrates the bubble train for a finite distance, but not over the whole train. Moreover, this distance, which is measured here by  $N_{\text{cor}}$ , decreases with increasing  $\mu$  and  $K$ . Perhaps the nonuniqueness of the solution to problems (13)–(15) may be attributed to the finiteness of the correlation length of the system. Indeed, if we have no correlations between bubbles, then the various states under the same pressure drop, but with different domain structure, may be considered as equivalent compositions of the independent bubble blocks. This agrees with the behavior of bubble chains at a large  $\mu K$ , when chaotic structures of bubble chains indicate the weak correlation between neighboring bubbles. There is another reason for the appearance of randomization in the train. If  $N$  exceeds the correlation length  $N_{\text{cor}}$ , then various parts of the train become ‘‘independent.’’ The local structure of the train can vary irregularly with  $\rho_{N-1}$ , i.e., the free tail of the train does not

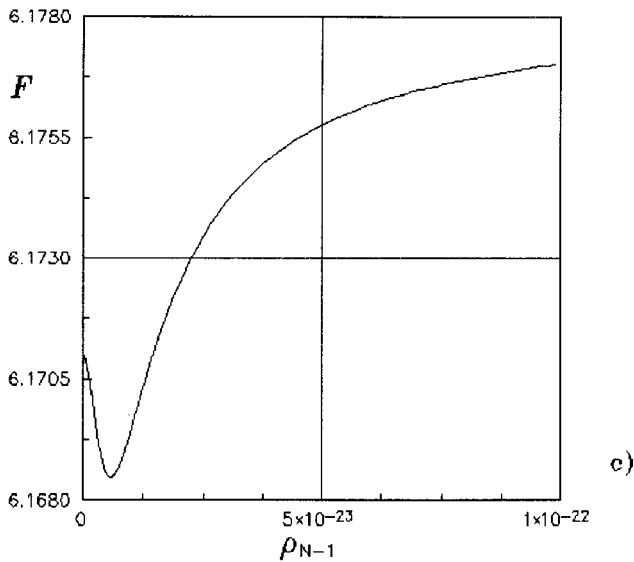
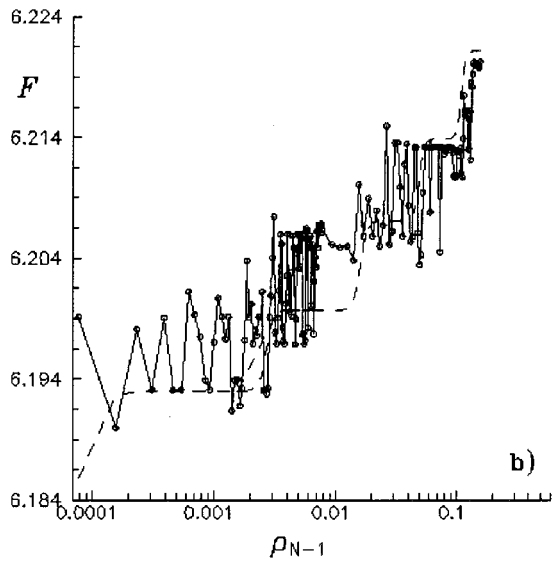
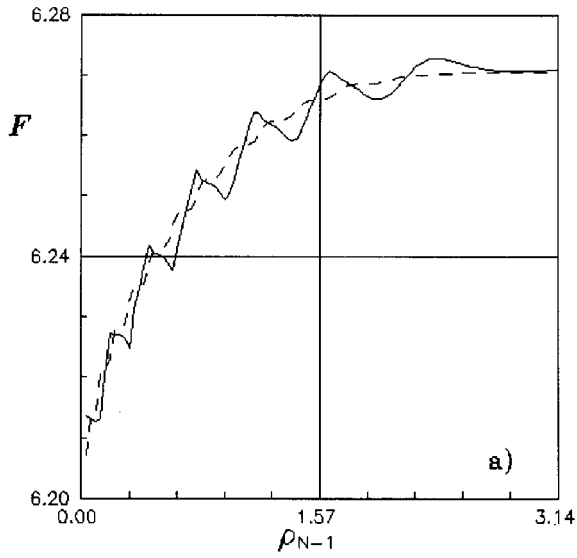


FIG. 9. The energy  $F$  associated with the states in Fig. 8. Dashed lines represent the respective dependence based on the continuous model.

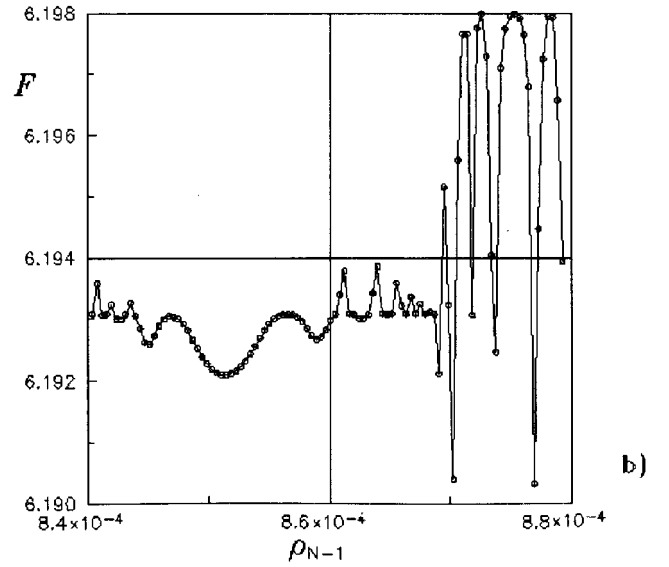
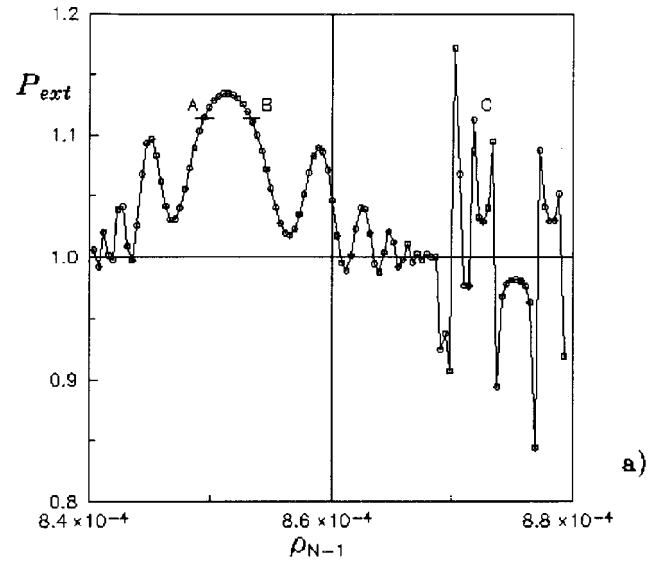


FIG. 10. (a) The external pressure and (b) the associated energy for the states from stochastic layer,  $\mu=0.008$ ,  $K=1$ ,  $N=101$ .

“feel” the events at the loaded end. The mathematical origin of this fact consists in the presence of a thin stochastic layer at the vicinity of the separatrix, even for a small  $K\mu$  [24]. If the trajectory starts from the vicinity of hyperbolic point  $\rho_{N-1} \rightarrow 0$ , then such a trajectory will pass through the stochastic layer by clinging to the separatrix.

It would be useful to estimate the number of the bubbles over which the load is distributed entirely. We apply the continuous model for such an estimate, because in most applications parameter  $\mu$  is very small. By integrating Eqs. (23) and (24), we arrive at the solution [18]

$$L = 2\pi KN = \int_1^{P_{\text{ext}}} dp \left( P_m^* - \ln P_m^* - 1 - \ln \frac{p}{P_m} - P_m + p \right)^{-1/2} \times \left( \ln \frac{p}{P_m} - P_m - p \right)^{-1/2}, \quad (32)$$

where  $P_m^* = P_m^*(\mu, K)$  is the maximum pressure prescribed to the separatrix,  $P_m$  is the maximum pressure for a given tra-

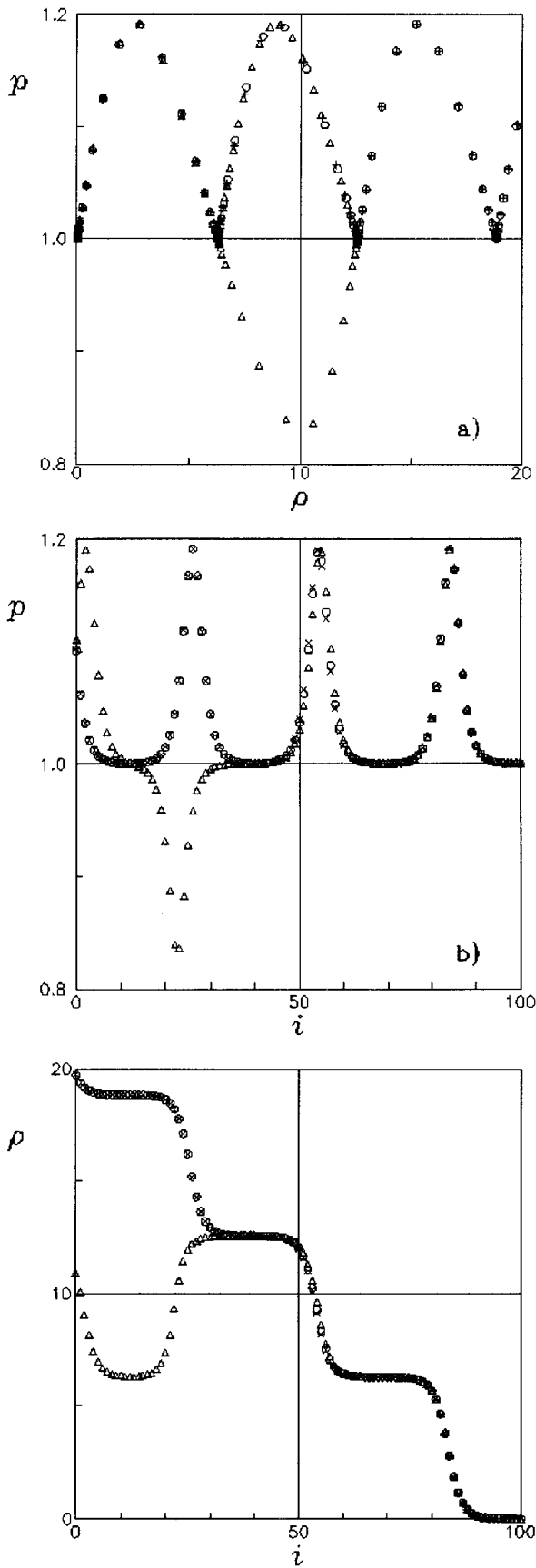


FIG. 11. (a) The phase portrait, (b) the pressure distribution over the train, and (c) the lamella displacement for states A( $\circ$ ), B( $+$ ), and C( $\Delta$ ) corresponding to Fig. 10(a).

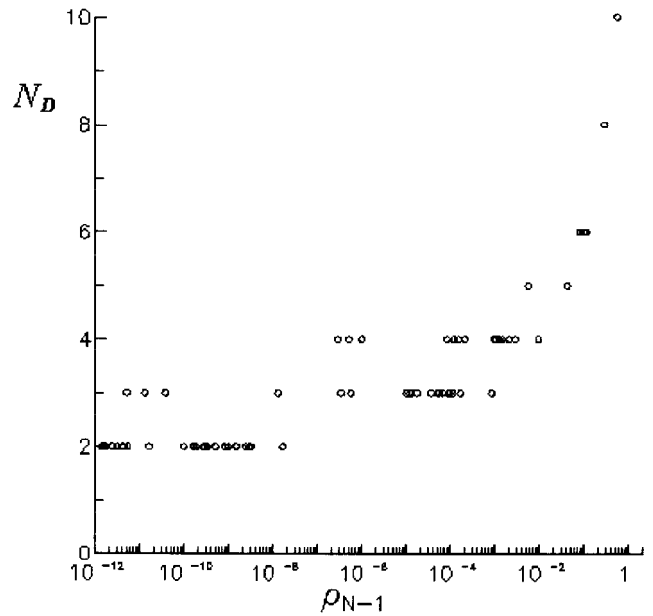


FIG. 12. The number of domains,  $N_D$ , as a function of the displacement of the last lamella for the states prescribed to  $P_{\text{ext}} = 1.1$  and  $\mu = 0.008$ ,  $K = 1$ ,  $N = 101$ .

jectory that is attributed to point ( $\rho = \pi$ ), and  $P_{\text{ext}}$  is the applied pressure associated with the desired length of the bubble train (Fig. 15). Analysis of the integral shows that the number of lamellae in the train rises as  $P_{\text{ext}}$  tends to  $P_m$ , and the respective trajectory goes in the vicinity of the separatrix. Contrarily, if  $L \rightarrow 0$ , the applied pressure is expected to be smaller than  $P_m$ . In most applications, parameter  $\mu/K$  is small. Hence,  $P_m^* \sim 1$ , and we can use the asymptotic expansion with respect to  $P_{\text{ext}} - 1$ . In the new variables  $x = p - 1$ ,

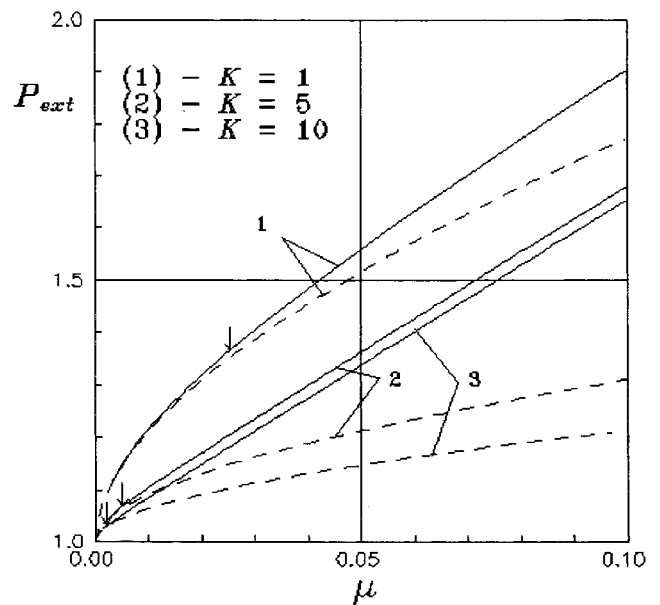


FIG. 13. The maximum pressure  $P_{\text{ext}}$  as it might be expected for “adiabatic” loading,  $N = 101$ . Dashed lines represent theoretical dependence (29). The arrows point out the critical parameters defined by Eq. (22).

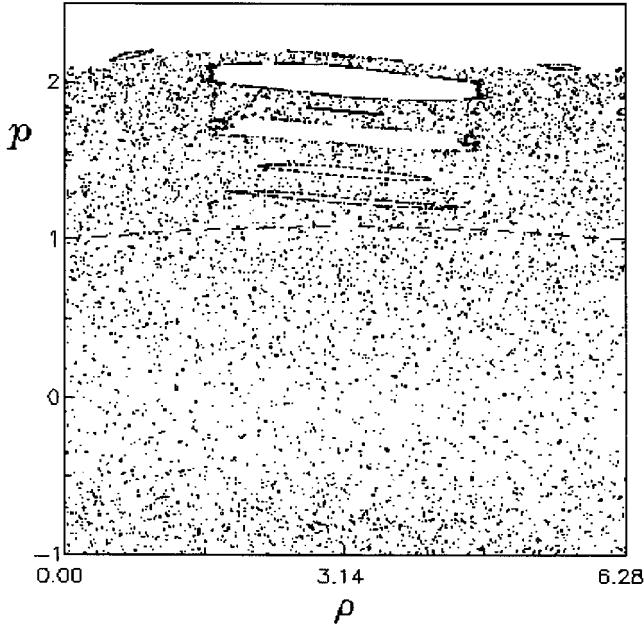


FIG. 14. The typical phase portrait for discrete map (13) and (14),  $\mu=0.016$ ,  $K=10$ ,  $N=2000$  and six starting points. A dashed line represents the separatrix of the continuous model, Eq. (26).

$x_{\text{ext}}=P_{\text{ext}}-1$ ,  $x_m=P_m-1$ , and  $x_m^*=P_m^*-1$ , we rewrite Eq. (32) with quadratic accuracy as

$$\frac{Lx_m^*}{2} \approx \int_0^\epsilon \frac{d\theta}{\sqrt{(k^2-\theta^2)(1-k^2+\theta^2)}}, \quad (33)$$

where  $k=x_m/x_m^*$  and  $\epsilon=x_{\text{ext}}/x_m^*$ . Integral (33) can be expressed through the Jacobi elliptic functions so that we find the external pressure drop as a function of arlength, namely,

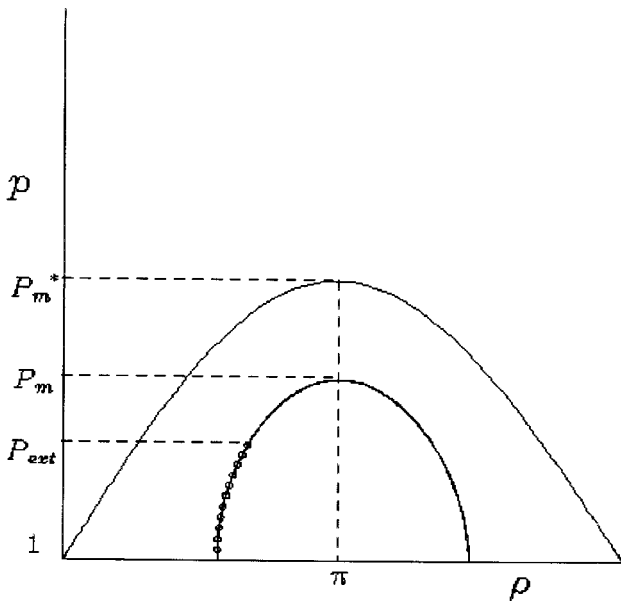


FIG. 15.  $P_m^*=P_m^*(\mu, K)$  is the maximum pressure prescribed to the separatrix,  $P_m$  is the maximum pressure for a given trajectory, and  $P_{\text{ext}}$  is the applied pressure associated with given length of the bubble train.

$$x_{\text{ext}}=x_m^* \frac{k\sqrt{1-k^2} \operatorname{sn}(Lx_m^*/2, k)}{\sqrt{1-k^2} \operatorname{sn}(Lx_m^*/2, k)}. \quad (34)$$

The extremalization of Eq. (34) gives us parameter  $k=k_m$ . Then we can find the desired dependence  $x_{\text{ext}}(L, x_m^*)$ . It is very difficult to study this dependence analytically, but qualitative estimates can be reached.

First of all, as  $Lx_m^*/2$  tends to infinity, parameter  $x_{\text{ext}}$  reaches  $x_m$ , i.e.,  $k=\epsilon$  so that the right-hand side of Eq. (34) tends to a constant that does not depend upon  $Lx_m^*/2$ . This saturation effect demonstrates the formation of a domain wall within an infinitely long chain, like that expressed by Eq. (28) [26]. A simple estimate for the critical pressure drop can be found by taking the limit  $\mu/K \rightarrow 0$  in Eq. (29). In the dimensional form, this start-up yield pressure drop  $\bar{G}$  is written as

$$\bar{G}=4\sqrt{P_g \sigma \delta / r_0 \lambda K}. \quad (35)$$

Contrarily, if  $Lx_m^*/2$  is small, then the elliptic function may be represented analytically [32], and the extremalization of Eq. (33) results in root  $k=1/\sqrt{2}$ . Therefore, in this limit

$$x_{\text{ext}}=x_m^* \frac{Lx_m^*}{4}. \quad (36)$$

Taking into account that for small  $\mu$  the asymptotic expression  $x_m^* \sim \sqrt{\mu/K}$  holds [26], from Eq. (36) we obtain

$$x_{\text{ext}} \sim N\pi\mu/2K, \quad (37)$$

and in the dimensional form Eq. (37) is written as

$$\bar{G} = \frac{2\pi\sigma\delta}{Kr_0\lambda} N. \quad (38)$$

The linearity of function  $\bar{G}(N)$  displays the independence of contributions of each lamella into the total pressure drop. This behavior might be expected for two limiting cases of the gas state in foam. If the gas in the bubbles were absolutely compressible, then the start-up yield pressure drop is completely determined by the overall Laplacian barrier. In the opposite limit, i.e., for an absolutely incompressible gas, one expects the similar linear behavior of the critical pressure drop.

Thus, the two limiting regimes expressed by Eqs. (35) and (38) facilitate the treating of experimental data and demonstrate the importance of the scales under consideration. So, if we use the short models, the critical pressure drop will depend upon the length of the sample, regardless of the foam texture. At the same time, one expects that field pilot experiments will demonstrate the universal character of the critical pressure drop versus input physical parameters. In Fig. 16, the experimental data reported by Falls, Musters, and Ratulowski [7] (their Table 2) are fitted into formula (38) ( $G \sim r_b^{-3}$ ,  $r_b$  is the effective radius of a bubble), where the number of lamellae per unit length is inversely proportional to the volume of gas per bubble [3]. In the same picture, the expected result for a long train is presented as line 1, Eq. (35) ( $G \sim r_b^{-3/2}$ ). Since the number of lamellae in the caravan was

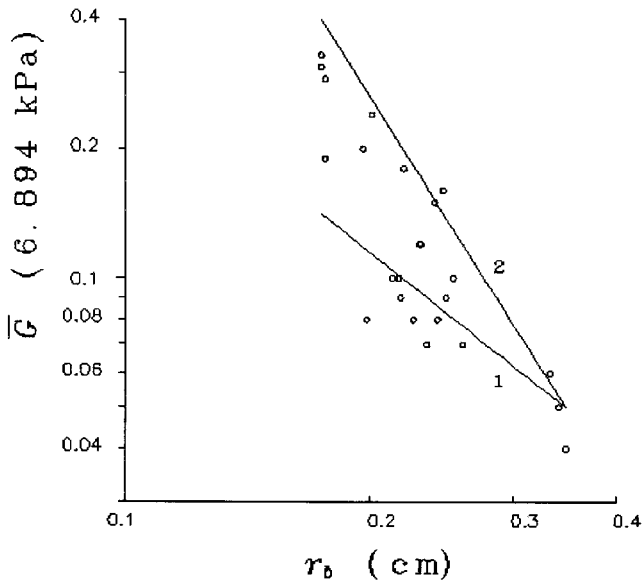


FIG. 16. Log-log plot of the critical pressure drop as a function of the effective bubble radius  $r_b$ . Experimental points [7] (○) are fitted into Eq. (35), line 1, and Eq. (38), line 2, by making use of the three last points  $r_b \rightarrow 0.4$ .

approximately eight, formula (38) is suitable and describes the experiment well. The correlation length covers the bubble train as a whole here.

## VII. CONCLUSIONS

The obtained results show that the character of the distribution of pressures  $p_i$  and displacements  $\rho_i$  for a bubble chain in a steady state depends upon the product  $\mu K$ , i.e., upon the measure of pinning energy with respect to the binding energy per unit link. For  $\mu K$  smaller than a critical value as defined by Eq. (30), various characteristics of the chain are well predicted by the continuous model. The pressure  $P_{\text{ext}}$ , which a bubble chain withstands in a steady state, cannot exceed  $P_{\text{max}}$ , the maximum pressure attributed to a given  $\mu$  and  $K$ . For any  $P_{\text{ext}} \leq P_{\text{max}}$ , a unique distribution of  $p_i$  and  $\rho_i$  forms in the chain with a given  $N$ .

When  $\mu K$  varies near its critical value, Eq. (30), the system (13) and (14) has several solutions with a given  $P_{\text{ext}}$  and with a small energy difference. A specific class of solutions can be found by applying the so-called principle of adiabatic transition. Namely, by imposing a crystalline structure to the initial unperturbed state of a chain, the simplest domain structure can be obtained by slowly increasing the applied pressure  $P_{\text{ext}}$ . However, for a large  $\mu K$  [see Eq. (30)], the principle of adiabatic transition from the initial uncharged state to that under pressure  $P_{\text{ext}}$  breaks, because there are such steady states that cannot be obtained by simply increasing  $P_{\text{ext}}$ .

Anyway, for each given  $\mu$ ,  $K$ , and  $N$ , the bubble train is able to withstand only a load bounded from above. Such maximum pressure  $P_{\text{ext}}$  is specified for each given set of input parameters. At larger pressures, one expects that the system begins motion, and a dynamic model is needed to describe such behavior. The dynamic effects might be sig-

nificant, even for smaller applied pressures, if the system resides in a metastable state.

The history of loading is very important for foam patterning. In particular, as it follows from the numerical experiments, the adiabatic transition from crystallinelike order to glasslike ordering cannot happen monotonically. At the same time, since the glasslike ordering improves the effect of foam screening, it would be highly desirable to clarify the regimes of loading that result in the coarse-grained foam superstructure. This superstructure might be imagined as a random system of blocks with internal crystallinelike order, separated by domain walls. In other words, the domain walls serve as apparent lamellae, and the blocks play the role of gas bubbles. To reinstate flow, the “yield” pressure drop has to overcome the initial start-up critical pressure drop. It was typically 10%–20% larger than that required to keep the lamellae moving [33]. This fact qualitatively agrees with the theoretical predictions discussed above.

In recent years, much attention has been paid to the dynamic behavior of systems possessing many metastable states [34,35]. As a rule, various modifications of the cellular-automaton model have been used for numerically simulating such systems [34,36]. One expects that the dynamics of the bubble trains moving through the network of active channels will demonstrate the characteristic features of self-organized criticality. The expectations are supported, in particular, by recent analysis of mathematically similar problems [37,38].

## ACKNOWLEDGMENTS

It is a great pleasure for us to thank Professor G. M. Homsy, from Stanford University, and Professor J. Ockendon, from Oxford University, for fruitful discussions. We also would like to express appreciation to Professor E. V. Teodorovich (IPM RAN) for encouragement in this work. We are grateful to S. Spears for giving a critical reading of the manuscript.

## APPENDIX: CALCULATION OF BUBBLE VOLUME

Consider the variation of bubble volume  $\Delta V_i$  caused by displacement of the  $i$ th lamella. This variation may be subdivided into two parts [we follow notations in Fig. 1(b)]. The first is the volume  $\Delta V_i'$  bounded by capillary walls between two cross sections at point  $x = \lambda/2$  and at point  $x = a_i$ . The second volume  $\Delta V_i''$  is bounded by a chord at point  $x = a_i$  and the spherical midsurface of the lamella. These two volumes can be expressed as

$$\Delta V_i' = \pi \int_{\lambda/2}^{a_i} \left( r_0 + \delta \cos \frac{2\pi x}{\lambda} \right)^2 dx, \quad \Delta V_i'' = \pi \int_{a_i}^{x_m} h^2(x) dx, \quad (\text{A1})$$

where the function  $h(x)$  can be written as

$$h = R \sin \varphi, \quad R - R \cos \varphi = x_m - x, \quad 0 \leq \varphi \leq \alpha. \quad (\text{A2})$$

Here  $R$  is the radius of lamella, and  $x_m$  is the intersection point of the membrane and axis  $x$ .

Simple algebra gives us the resulting variation of bubble volume in the following form:

$$\begin{aligned} \Delta V_i = \Delta V_i' + \Delta V_i'' = \pi \left( a_i - \frac{\lambda}{2} \right) \left( r_0^2 + \frac{\delta^2}{2} \right) \\ + \lambda \delta r_0 \sin \frac{2\pi a_i}{\lambda} \left( 1 + \frac{\delta}{4r_0} \cos \frac{2\pi a_i}{\lambda} \right) \\ + \frac{\pi(x_m - a_i)^2}{3} (3R - x_m + a_i). \end{aligned} \quad (\text{A3})$$

Substituting  $\varphi = \alpha$  into Eq. (A2), we find

$$R = \frac{r_0 + \delta \cos 2\pi a_i / \lambda}{\sin \alpha}, \quad x_m = a_i + R(1 - \cos \alpha), \quad (\text{A4})$$

where the angle  $\alpha$  can be obtained by using the assumption (5):

$$\tan \alpha = \left. \frac{dr}{dx} \right|_{x=a_i} = -\frac{2\pi\delta}{\lambda} \sin \frac{2\pi a_i}{\lambda}. \quad (\text{A5})$$

Thus, the volume  $\Delta V_i$  can be expressed in terms of  $a_i$ . Making use of assumption (2) ( $\delta/\lambda \ll 1$ ), we obtain

$$\alpha \approx \sin \alpha \approx \tan \alpha \approx -\frac{2\pi\delta}{\lambda} \sin \frac{2\pi a_i}{\lambda}, \quad \cos \alpha \approx 1. \quad (\text{A6})$$

Substituting Eqs. (A4)–(A6) into (A3), we find

$$\Delta V_i = \pi \left( a_i - \frac{\lambda}{2} \right) \left( r_0^2 + \frac{\delta^2}{2} \right) + \left[ \lambda \delta r_0 \left( 1 + \frac{\delta}{4r_0} \cos \frac{2\pi a_i}{\lambda} \right) - \frac{\pi^2 r_0^3 \delta}{2\lambda} \left( 1 + \frac{3\delta}{r_0} \cos \frac{2\pi a_i}{\lambda} \right) \right] \sin \frac{2\pi a_i}{\lambda}. \quad (\text{A7})$$

It is convenient to rewrite Eq. (A7) in the form of an expansion with respect to the small parameters  $\delta/r_0 \ll 1$  and  $r_0/\lambda \ll 1$ . Substituting argument  $a_i - \lambda/2$  into sinus in the right-hand side of Eq. (A7), instead of  $a_i$ , we find

$$\begin{aligned} \Delta V_i = \pi \left( a_i - \frac{\lambda}{2} \right) r_0^2 \left\{ 1 - \frac{2\delta}{r_0} \frac{\sin[2\pi(a_i - \lambda/2)/\lambda]}{[2\pi(a_i - \lambda/2)/\lambda]} \right\} \\ + \pi \left( a_i - \frac{\lambda}{2} \right) r_0^2 \left\{ \frac{\delta^2}{2r_0^2} - \frac{\sin[2\pi(a_i - \lambda/2)/\lambda]}{[2\pi(a_i - \lambda/2)/\lambda]} \left[ \frac{\delta^2}{2r_0^2} \cos \frac{2\pi a_i}{\lambda} - \frac{\pi^2 r_0 \delta}{\lambda^2} \left( 1 + \frac{3\delta}{r_0} \cos \frac{2\pi a_i}{\lambda} \right) \right] \right\}. \end{aligned} \quad (\text{A8})$$

For our goals, we need only the principal term of this expansion. It has the form

$$\Delta V_i = \pi r_0^2 \left( a_i - \frac{\lambda}{2} \right). \quad (\text{A9})$$

Then the volume of the bubble as a whole becomes

$$V_i = \pi r_0^2 (a_i - a_{i-1}). \quad (\text{A10})$$

- 
- [1] *Foams: Physics, Chemistry and Structure*, edited by A. J. Wilson (Springer-Verlag, Berlin, 1989).
- [2] R. J. Treinen, W. E. Brigham, and L. M. Castanier (unpublished).
- [3] G. Hirasaki and J. Lawson, Soc. Petr. Eng. J. **25**, 176 (1985).
- [4] S. S. Marsden (unpublished).
- [5] G. R. Assar and R. W. Burley, in *Encyclopedia of Fluid Mechanics*, edited by N. P. Cheremisinoff (Gulf Coleman, Houston, 1886), Vol. 3, pp. 26–42.
- [6] A. M. Kraynik, Annu. Rev. Fluid Mech. **20**, 325 (1988).
- [7] A. H. Falls, J. J. Musters, and J. Ratulowski, SPE Reserv. Eng. **4**, 55 (1989).
- [8] A. R. Kovscek and C. J. Radke, in *Foams: Fundamentals and Applications in the Petroleum Industry*, Advances in Chemistry Series No. 242, edited by L. L. Schramm (American Chemical Society, New York, 1994), pp. 115–164.
- [9] J. E. Hanssen and M. Dalland, in *Foams: Fundamentals and Applications in the Petroleum Industry* (Ref. [8]), pp. 319–354.
- [10] W. R. Rossen, in *Foams: Theory, Measurements and Applications*, edited by R. K. Prud'homme and S. A. Khan, Surfactant Science Series (Marcel Dekker, New York, 1995), Vol. 57, pp. 413–464.
- [11] C. W. Nutt and R. W. Burley, in *Foams: Physics, Chemistry and Structure* (Ref. [1]), pp. 105–147.
- [12] R. W. Flumerfelt and J. Prieditis, in *Surfactant-Based Mobility Control: Progress in Miscible-Flood Enhanced Oil Recovery*, ACS Symposium Ser. 373, edited by D. H. Smith (ACS, Washington, D.C., 1988), pp. 295–325.
- [13] W. R. Rossen, J. Colloid Interface Sci. **136**, 1 (1990).
- [14] P. G. de Gennes, Rev. Inst. Fr. Pet. **47**, 249 (1992).
- [15] W. R. Rossen, J. Colloid Interface Sci. **136**, 17 (1990); **136**, 38 (1990); **139**, 457 (1990).
- [16] Y. I. Frenkel and T. A. Kontorova, Zh. Eksp. Teor. Fiz. **8**, 1340 (1938).
- [17] B. D. Josephson, Adv. Phys. **14**, 419 (1965).
- [18] A. Seeger and P. Schiller, in *Physical Acoustics*, edited by W. P. Mason and R. N. Thurston (Academic, New York, 1966), Vol. IIIA, p. 361.
- [19] I. O. Kulik, Zh. Eksp. Teor. Fiz. **51**, 1952 (1966) [Sov. Phys. JETP **24**, 1307 (1967)].

- [20] A. Barone and G. Paterno, *Physics and Applications of the Josephson Effect* (John Wiley and Sons, New York, 1982).
- [21] P. Bak, *Rep. Prog. Phys.* **45**, 587 (1982).
- [22] J. Lowell, *J. Phys. F* **8**, 501 (1978).
- [23] W. R. Rossen and P. A. Gauglitz, *AIChE. J.* **36**, 1176 (1990); V. M. Entov and R. G. Musin (unpublished).
- [24] M. A. Lieberman and A. J. Lichtenberg, *Phys. Rev. A* **5**, 1852 (1972).
- [25] A. J. Lichtenberg and M. A. Lieberman, *Regular and Chaotic Dynamics*, 2nd ed. (Springer-Verlag, New York, 1992).
- [26] K. G. Kornev, *Zh. Eksp. Teor. Fiz.* **107**, 1895 (1995) [*JETP* **80**, 1049 (1995)].
- [27] K. T. Chambers and C. J. Radke, in *Interfacial Phenomena in Petroleum Recovery*, edited by N. Morrow (Marcel Dekker Inc., New York, 1990), pp. 191–255.
- [28] O. S. Owete and V. E. Bringham, *SPE Res. Eng.* **2**, 315 (1987).
- [29] A. Bazilevsky, K. Kornev, and A. Rozhkov, in *Proceedings of the ASME Symposium on Rheology & Fluid Mechanics of Nonlinear Materials, Atlanta, 1996* (ASME, New York, in press).
- [30] K. G. Kornev and V. N. Kurdyumov, *Zh. Eksp. Teor. Fiz.* **106**, 457 (1994) [*JETP* **79**, 252 (1994)].
- [31] E. V. Teodorovich (private communications); Ch. Kittel, *Introduction to Solid State Physics* (John Wiley and Sons, New York, 1956).
- [32] *Handbook of Mathematical Functions*, edited by M. Abramowitz and I. A. Stegun (Dover, New York, 1965).
- [33] R. A. Albrecht and S. S. Marsden, *Soc. Petr. Eng. J.* **10**, 51 (1970).
- [34] P. Bak, C. Tang, and K. Wiesenfeld, *Phys. Rev. A* **38**, 364 (1988).
- [35] P. Bak and K. Chen, *Sci. Am.* **264** (1), 26 (1991).
- [36] W. G. Laidlaw, W. G. Wilson, and D. A. Coombe, *Can. J. Chem.* **70**, 482 (1992).
- [37] S. A. Ginsburg, *Zh. Exp. Teor. Fiz.* **106**, 607 (1994) [*JETP* **79**, 334 (1994)].
- [38] F. Marchesoni and M. Patriarca, *Phys. Rev. Lett.* **72**, 4101 (1994).